ELSEVIER

Chemical Engineering Journal 127 (2007) 23–30

Chemical Engineering Journal

www.elsevier.com/locate/cej

An experimental evaluation of state estimation with fluid dynamical models in process tomography

Aku Seppänen [a], Lasse Heikkinen [a], Tuomo Savolainen [a], Arto Voutilainen [a,*], Erkki Somersalo [b], Jari P. Kaipio [a]

[a] *Department of Physics, University of Kuopio, P.O. Box 1627, FIN-70211 Kuopio, Finland*
[b] *Institute of Mathematics, Helsinki University of Technology, P.O. Box 1100, FIN-02015 TKK, Finland*

Received 6 October 2005; received in revised form 31 August 2006; accepted 22 September 2006

Abstract

In this paper we perform an experimental evaluation of a state estimation approach in process tomography. In particular, we concentrate on the case where a system with rapidly moving target is imaged with electrical impedance tomography. We show experimental results which confirm that non-stationary estimation with proper fluid dynamical models works well even in cases where stationary estimates are completely useless.

Keywords: Process tomography; Electrical impedance tomography (EIT); State; Estimation

1. Introduction

In process tomography the aim is to monitor industrial processes on the basis of indirect observations from the boundary of the target. Techniques used in process monitoring are basically the same as in medical imaging. The variety of modalities include electrical, optical, X-ray and nuclear tracer techniques. In many applications one is often interested in imaging targets that change very rapidly. That is the case for example in mixing [1–3] and mass transport [4–6] applications. If the target changes at a very high rate in comparison with the rate of measurements, the stationary tomographic reconstructions are usually inadequate. In such cases the reconstructions may be improved by using the state estimation approach [7]. In state estimation approaches the temporal behavior of the target is modeled and the model is used in the image reconstruction to provide further information on the target.

In [8,9] we applied the state estimation approach to electrical impedance tomography (EIT) in the case of moving fluids. We modeled the dynamics of the system using the Navier–Stokes equations and the convection–diffusion (CD) equation. The resulting stochastic evolution model together with the observation model of EIT constituted the state-space representation of the system. The reconstruction of conductivity distributions was based on this representation, and the algorithms used in the image reconstruction were of the Kalman Filter type. The cited numerical studies have shown that the use of state estimation with suitable evolution models may improve the estimates considerably.

The aim of this paper is to provide an experimental validation of the state estimation approach in EIT. State estimation has already been applied to real EIT data in papers [10–12]. However, in these papers the random walk model has been used as the evolution model, instead of more realistic models.

In this paper we consider an experimental EIT measurement set up consisting of a saline-filled tank with a rotating impeller and a saline-filled table tennis ball floating in the tank. EIT measurements are carried out and the state estimation approach with an appropriate evolution model is used in the reconstruction of the conductivity distribution within the tank. The evolution model is based on approximate fluid dynamical modeling of the system and on a convection–diffusion model. The time-dependent internal structure, i.e. the impeller, is also taken into account in the reconstruction.

2. State estimation in EIT

In EIT conductive targets are monitored using electrical boundary measurements. Electric current is injected into the

* Corresponding author.
E-mail address: Arto.Voutilainen@uku.fi (A. Voutilainen).

1385-8947/$ – see front matter © 2006 Elsevier B.V. All rights reserved.
doi:10.1016/j.cej.2006.09.025

target using electrodes attached to the boundary of the target. The resulting voltages between the electrodes are measured and the internal conductivity distribution is reconstructed on the basis of the voltage measurements.

The reconstruction problem has a nature of an ill-posed inverse problem – even in a stationary case – and hence special estimation methods and appropriate modeling of the measurements are always required. An additional difficulty arises from time-varying targets because the voltage measurements at different times do not correspond to the same target. Hence, the use of data corresponding to multiple current injection patterns may lead to severe inaccuracies. On the other hand, when using ordinary (stationary) reconstruction algorithms, a single current injection does not (usually) yield adequate information for reconstructing the conductivity distribution. In order to tackle the problem of non-stationarity, we write EIT in state-space formalism, and utilize fluid dynamical modeling in the reconstruction.

In Section 2.1 we review the observation model of EIT. We also point out the difference between the stationary and the non-stationary reconstruction problems. In Section 2.2 we introduce one fluid dynamical model, the convection–diffusion model, which is used for modeling the time-dependence of the target in this paper. Finally, in Section 2.3 we write the reconstruction problem of EIT in the form of a state estimation problem and introduce two algorithms, Kalman filter and fixed-lag Kalman smoother that can be used for solving the problem.

2.1. Observation model

In EIT, alternating currents I_ℓ are applied to electrodes on the surface of the object, and the resulting voltages between different pairs of electrodes are measured. The conductivity distribution σ within the object is reconstructed on the basis of the voltage measurements. We model the observations by using the complete electrode model (CEM) which is known to be so far the most accurate model used in EIT [13]. The CEM consists of the following equations:

$$\nabla \cdot (\sigma \nabla u) = 0, \quad x \in \Omega \tag{1}$$

$$u + z_\ell \sigma \frac{\partial u}{\partial n} = U_\ell, \quad x \in e_\ell, \quad \ell = 1, 2, \ldots, L \tag{2}$$

$$\int_{e_\ell} \sigma \frac{\partial u}{\partial n} \, \mathrm{d}S = I_\ell, \quad x \in e_\ell, \quad \ell = 1, 2, \ldots, L \tag{3}$$

$$\sigma \frac{\partial u}{\partial n} = 0, \quad x \in \partial\Omega \backslash \cup_{\ell=1}^{L} e_\ell \tag{4}$$

where $u = u(x)$ is the electric potential, e_ℓ the ℓth electrode, z_ℓ the contact impedance between the ℓth electrode and contact material, U_ℓ the potential on ℓth electrode, I_ℓ the injected current, n the outward unit normal and L is the number of the electrodes. In addition, the charge conservation law

$$\sum_{\ell=1}^{L} I_\ell = 0 \tag{5}$$

needs to be fulfilled. Further, in order to determine uniquely the potentials u and U_ℓ based on the CEM, the reference level of potential needs to be fixed. This is achieved, e.g. by writing

$$\sum_{\ell=1}^{L} U_\ell = 0 \tag{6}$$

We approximate the complete electrode model numerically using the finite element method (FEM), see [13–15]. The resulting finite dimensional observation model is of the form

$$V_t = U_t(\sigma_t) + \upsilon_t, \tag{7}$$

where t is a discrete time index, V_t the observed voltages resulting from one current injection pattern, $\sigma_t \in \mathbb{R}^{\mathrm{N}}$ a finite-dimensional approximation of the conductivity distribution at time t, $U_t(\sigma_t)$ a non-linear mapping between the conductivity and voltages and υ_t is observation error. If we further linearize the observation model (7) we obtain

$$V_t = U_t(\sigma_*) + J_t(\sigma_t - \sigma_*) + \upsilon_t, \tag{8}$$

where the matrix J_t is the Jacobian corresponding to the model $U_t(\sigma)$ and the vector σ_* is a linearization point.

In a *stationary case* it is assumed that the conductivity within the target does not change during the measurements, i.e., $\sigma_1 = \sigma_2 = \cdots = \sigma_{\mathrm{T}} =: \sigma$. Thus, the observation models corresponding to different current injection patterns $I_1, I_2, \ldots, I_{\mathrm{T}}$ can be combined into one stationary model

$$V = U(\sigma) + \upsilon, \tag{9}$$

where

$$V = \begin{bmatrix} V_1 \\ V_2 \\ \vdots \\ V_{\mathrm{T}} \end{bmatrix}, \qquad U(\sigma) = \begin{bmatrix} U_1(\sigma) \\ U_2(\sigma) \\ \vdots \\ U_{\mathrm{T}}(\sigma) \end{bmatrix} \quad \text{and} \quad \upsilon = \begin{bmatrix} \upsilon_1 \\ \upsilon_2 \\ \vdots \\ \upsilon_{\mathrm{T}} \end{bmatrix}. \tag{10}$$

Thus, in a stationary case the conductivity distribution σ is reconstructed based on the observation model (9). The reconstruction problem is known to be ill-posed, and hence spatial prior information of the target is needed to be utilized in the reconstruction. Spatial prior information is typically incorporated into the problem formulation by using the Tikhonov regularization scheme. The regularized solution is of the form

$$\widehat{\sigma} = \arg\min_{\sigma} \{||V - U(\sigma)||^2 + \alpha R(\sigma)\},$$

where $R(\sigma) > 0$ is a functional that favors certain *a priori* known features in the minimization and $\alpha > 0$ is a regularization parameter. The regularizing functional is usually selected as $R(\sigma) = ||L(\sigma - \sigma_{\mathrm{prior}})||^2$, where the regularization matrix L is typically a discrete differential operator, a choice which yields smooth estimates, and σ_{prior} is a prior guess for σ.

In the non-stationary case, however, the assumption that the conductivity distribution is non-varying during a set of different current patterns is no longer valid and therefore the stationary

observation model (9) cannot be used. Instead, it is necessary to use the time-dependent observation model (7) corresponding to a single current injection pattern only. As a consequence, the reconstruction problem is "even more ill-posed" than in the stationary case due to the small amount of data relative to the number of unknown parameters. Therefore, in order to obtain feasible reconstructions, we need more prior information of the target. In the state estimation approach we thus utilize information on the temporal behavior of the target. That is, we write a model for the time dependence of the target. In the case of moving fluid we can use fluid dynamical models, such as the Navier–Stokes equations and the convection–diffusion equation.

2.2. Evolution model

State estimation with fluid dynamical models in EIT has been described in [8,9]. In the case of moving fluid we use the convection–diffusion model

$$\frac{\partial c}{\partial t} = -\bar{v} \cdot \nabla c + \kappa \Delta c. \tag{11}$$

where c is the concentration of a substance, $\bar{v}$ the velocity and κ is the diffusion coefficient. The fluid velocity profile $\bar{v}$ can be obtained from measurements or from numerical modeling of the flow. In this study an approximate velocity profile is obtained as a solution of the Navier–Stokes equations

$$\rho \frac{\partial \bar{v}}{\partial t} + \rho \bar{v} \cdot \nabla \bar{v} - \mu \nabla^2 \bar{v} + \nabla p = \rho \bar{g} \tag{12}$$

$$\frac{\partial \rho}{\partial t} + \nabla \cdot \rho \bar{v} = 0. \tag{13}$$

We use FEM to approximate the solution of the Navier–Stokes equations and convection–diffusion equation. Furthermore, we assume that the dependence between the conductivity and the concentration is linear. With this choice the FEM scheme leads to a discrete-time evolution model in terms of conductivity

$$\sigma_{t+1} = F_t \sigma_t + s_{t+1} + w_{t+1}, \tag{14}$$

where F_t is called the state transition matrix, and the vector s_{t+1} is a source term which depends on the boundary conditions of the CD equation. The vector w_t is called the state noise, which represents the inaccuracies/uncertainties of the model. For details of the numerical approximation of the CD equation, see [8,16]

2.3. State estimation

The approximate observation model (8) and evolution model (14) constitute the state-space model of the system. On the basis of this model we can pose the state estimation problem, which is of the form: Compute the conditional expectation of the random variable σ_t based on a set of observations $V_{1:k} = \{V_1, V_2, \ldots, V_k\}$, that is, $\sigma_{t|k} = E\{\sigma_t | V_{1:k}\}$. The estimates are sought by using recursive methods. For example, the on-line estimates $\sigma_{t|t}$ can be computed with the Kalman filter

$$\sigma_{t|t-1} = F_{t-1}\sigma_{t-1|t-1} + s_t \tag{15}$$

$$\Gamma_{t|t-1} = F_{t-1}\Gamma_{t-1|t-1}F_{t-1}^{\mathrm{T}} + \Gamma_{w_{t-1}} \tag{16}$$

$$K_t = \Gamma_{t|t-1}J_t^{\mathrm{T}}(J_t\Gamma_{t|t-1}J_t^{\mathrm{T}} + \Gamma_{v_t})^{-1} \tag{17}$$

$$\Gamma_{t|t} = (I - K_tJ_t)\Gamma_{t|t-1} \tag{18}$$

$$\sigma_{t|t} = \sigma_{t|t-1} + K_t(V_t - U_{0,t} - J_t(\sigma_{t|t-1} - \sigma_*)), \tag{19}$$

where Γ_{v_t} is the covariance of the observation noise, Γ_{w_t} the covariance of the state noise and the conditional covariances are defined as $\Gamma_{t|k} = \mathrm{cov}\{\sigma_t - \sigma_{t|k}, \sigma_t - \sigma_{t|k}\}$. Furthermore, the estimates $\sigma_{t|k}$, $k > t$ can be computed with the (fixed-lag or fixed-interval) Kalman smoother [17]. Generally, the smoothers give better reconstructions because they also utilize the future observations when computing the conductivity corresponding to time t. In fixed-lag smoothing the objective is to compute the expectations $\sigma_{t-q|t}$ $q > 0$. The fixed-lag Kalman smoother is of the form

$$K_{t-i} = \Gamma_{t|t-1}^{(i,0)}J_t^{\mathrm{T}}(J_t\Gamma_{t|t-1}J_t^{\mathrm{T}} + \Gamma_{v_t})^{-1}, \quad i = 0, \ldots, q \tag{20}$$

$$\sigma_{t-i|t} = \sigma_{t-i|t-1} + K_{t-i}(V_t - U_{0,t} - J_t(\sigma_{t-i|t-1} - \sigma_*)), \quad i = 0, \ldots, q \tag{21}$$

$$\Gamma_{t+1|t}^{(i+1,0)} = \Gamma_{t|t-1}^{(i,0)}(I - K_tJ_t)^{\mathrm{T}}F_t^{\mathrm{T}}, \quad i = 0, \ldots, q \tag{22}$$

where the covariances $\Gamma_{t|t-1}^{(i,0)}$ are defined as

$$\Gamma_{t|t-1}^{(i,0)} = \mathrm{cov}\{\sigma_{t-i} - \sigma_{t-i|t-1}, \sigma_{t-i} - \sigma_{t-i|t-1}\}. \tag{23}$$

Thus, $\Gamma_{t|t-1}^{(0,0)} = \Gamma_{t|t-1}$ is obtained from the filter Eq. (16).

3. Experiments

In this section we describe the measurements that were carried out in order to evaluate the non-stationary estimation methods described in the previous section. The EIT measurements were performed in a flat cylindrical tank filled with saline. The contents of the tank were stirred with an impeller. Fig. 1 is a snapshot of a video recorded during the measurements. The white circle in Fig. 1 is a saline-filled table tennis ball (diameter 2.8 cm) floating in saline. The main objective of the experiment was to track the path of the ball based on EIT measurements, and to compare the result with the correct path seen in the videotape.

The height of the tank was 7 cm, and the diameter was 28 cm. The tank was covered with a transparent plastic cap, in order to prevent the shape of the saline surface to change due to centrifugal force. The impeller was rotated by an electric motor. The angular velocity of the impeller was constant; the time of rotation was 1.468 seconds. The measurements were performed by using the EIT equipment developed in the University of Kuopio [18]. We used 16 electrodes for the EIT measurements. The whitish rectangles on the boundary of the tank in Fig. 1 indicate the placement of the electrodes.

In the EIT measurements we used opposite current injections. However, in contrast to normal procedure, the currents were repetitively injected between the same pair of electrodes, instead

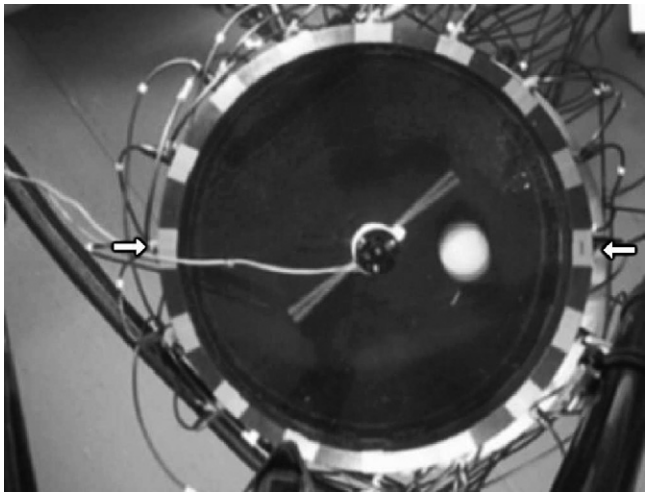

Fig. 1. Top view of the measurement setup. The arrows indicate the current-injecting electrodes.

of changing the current-carrying electrodes. The electrodes used for current injection are shown in Fig. 1. One of the current-injecting electrodes, the leftmost electrode, was also used as a ground electrode in the voltage measurements. In the stationary case the above choice of current injections would result poor reconstructions, because the repetition of the same current pattern does not yield further information on the structure of target. A traditional approach is to rotate the measurements around a stationary object. However, in our case the object rotates and the current injection pattern stays unchanged. Therefore, the selected current injection scheme corresponds (roughly) to a stationary situation in which the current-injecting electrodes are rotated on the boundary. The current injection was repeated 64 times, and the time between consecutive injections was 0.0557 s, on average. Thus, during 16 current injections – the number of injections typically needed for one stationary EIT reconstruction – the impeller rotated more than a half revolution. The amplitude of the injected alternating current was 1 mA. Corresponding to each current injection, voltages between 15 electrode pairs were measured: between one of the current-carrying electrodes and each of the other electrodes.

We also performed the EIT measurements corresponding to a stationary target. That is, we fixed the position of the impeller, and measured the voltages corresponding to one current injection. In this measurement the ball was not in the tank. This measurement was used for estimating the conductivities of the saline and the impeller. We first computed the best homogeneous estimate $\sigma_{\mathrm{bh}} \in \mathbb{R}$, i.e. a single value of conductivity obtained from least squares fitting. This estimate was used in the initialization of the computation of the linearization point. The conductivities of the impeller and saline were assumed to be uniform and the internal structure, i.e. the position of the impeller, was taken into account in the construction of σ_* [19].

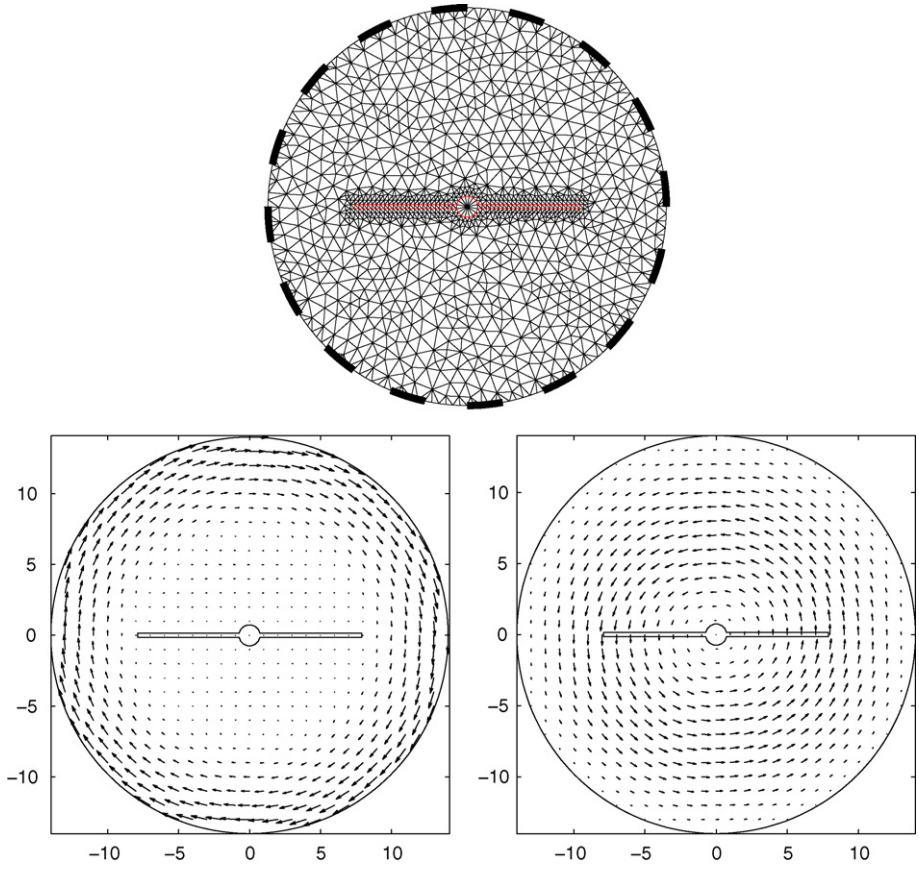

Fig. 2. Top: the finite element mesh. The thick lines on the boundary represent the electrodes. Bottom left: the velocity field used in the convection–diffusion model. The coordinate system is fixed to the impeller. The velocity field in the coordinate system fixed to the tank at one instant of time.

4. Convection–diffusion model

In this section we discuss the CD model used as the evolution model in state estimation. It is worth to notice that the CD model and the Navier–Stokes equations introduced below are *single-phase flow models*. This choice is of course contradictory with the fact that the actual target consists of two phases: the ball and saline. However, our previous results have indicated that the state estimates are relatively tolerant to inaccuracies in the flow model [21]. In the following sections we demonstrate experimentally that, indeed, the state estimates are quite feasible even if the flow model is inaccurate.

The CD model was formulated basically as described in Section 2. However, we had to modify our previous methods slightly because of the impeller. We modeled the impeller as an internal structure. We generated the finite element mesh taking into account the dimensions of the impeller (see Fig. 2). However, in order to utilize the information of the internal structure, we also needed the position of the impeller at the times of each current injection. In this study we simply checked the position of the impeller at the time of the first current injection in the video, and calculated the positions at the following time steps using our knowledge of the angular velocity of the impeller. We note that the position of the impeller could be determined in more sophisticated manner.

Since the impeller rotates, we would actually need different FE meshes for the different times. However, this need can be avoided by fixing the coordinates in the FE computations into the coordinates of the impeller. In the EIT model this required rotation of the electrode locations on the boundary of the mesh. The velocity field needed for the convection–diffusion model was computed numerically in coordinates fixed to the impeller. The Navier–Stokes equations were solved using the penalty method [20], i.e. the continuity Eq. (13) was replaced by

$$\nabla \cdot \bar{v} = -\frac{p}{\lambda}, \tag{24}$$

where λ is the penalty parameter and is set to be a large number. We approximated that the velocity field is stationary in the coordinates fixed to the impeller. Furthermore, when solving the Navier–Stokes equations, we ignored the centrifugal force and the Coriolis force that occur in the equations when performing the computations in rotating coordinates. However, when using state estimation we do not necessarily need a very accurate evolution model since our numerical studies have indicated that the estimation scheme is relatively tolerant to inaccuracies in the fluid dynamical models [21]. The computed velocity field is shown in Fig. 2.

The approximate model between subsequent conductivity distributions was obtained as a FE approximation of the CD model. Integration with respect to time was performed using the implicit Euler method. In order to avoid large inaccuracies, time interval between subsequent current injections was divided into multiple subintervals of equal length. In this case, the resulting multi-step model for the conductivities at the nodes outside the impeller is of the form (14) with $F_t = F^m$, where F is the state

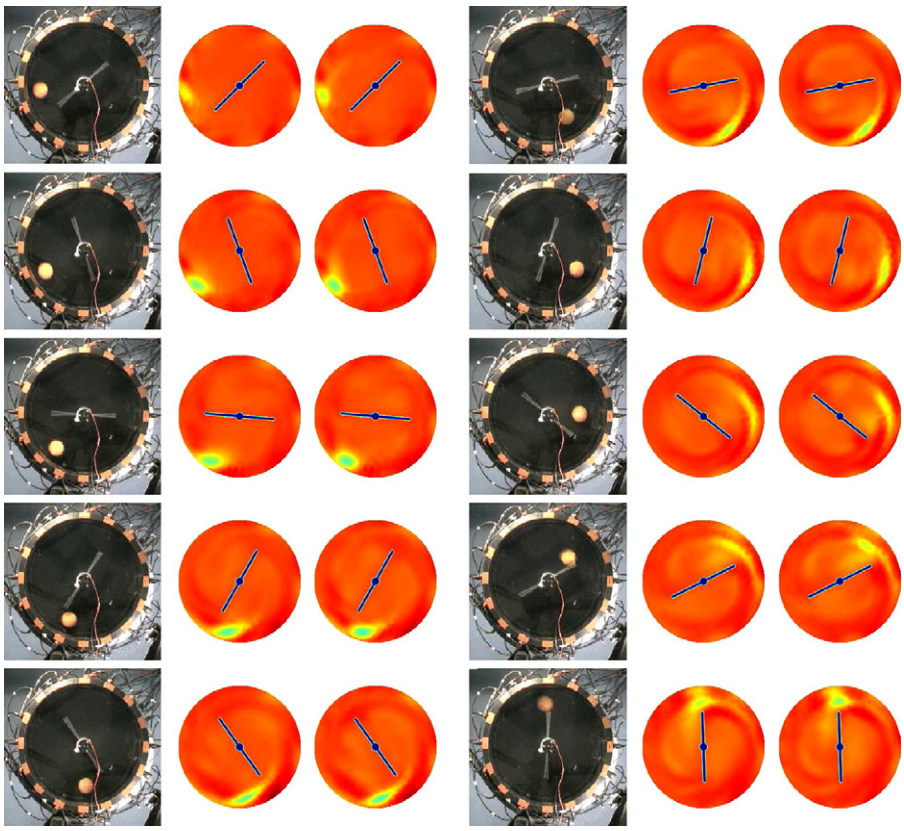

Fig. 3. The top views of the target (1st and 4th column), the Kalman filter reconstructions (2nd and 5th column), and the fixed-lag Kalman smoother reconstructions (3rd and 6th column).

transition matrix corresponding to one subinterval and m is the number of subintervals, and $s_t = 0$ since there is no input in the system.

5. Results

We computed the non-stationary EIT reconstructions using the fixed-lag Kalman smoother with lag $q = 8$. In the reconstruction we assumed that the conductivity was uniform throughout the impeller. Thus, the state to be estimated was $\sigma_t^{(\mathrm{r})} \in \mathbb{R}^M$, $M < N$, where the Mth element $\sigma_t^{(\mathrm{r})}(M)$ represented the conductivity of the impeller, and the elements $\sigma_t^{(\mathrm{r})}(1), \sigma_t^{(\mathrm{r})}(2), \ldots, \sigma_t^{(\mathrm{r})}(M-1)$ represented the conductivities at other nodal points of the mesh. The superscript (r) refers to the reduced dimensionality. The temporal evolution of the impeller conductivity was modeled as $\sigma_{t+1}^{(\mathrm{r})}(M) = \sigma_t^{(\mathrm{r})}(M) + \epsilon_t$, where the variance of the state noise ϵ_t was very small. Since the linearization point was the same at each time step, the quantity to be reconstructed was selected as $\tilde{\sigma}_t^{(\mathrm{r})} = \sigma_t^{(\mathrm{r})} - \sigma_*^{(\mathrm{r})}$. This choice does not cause any qualitative changes to the smoother equations. The fixed-lag smoother was initialized with $\tilde{\sigma}_{1|0}^{(\mathrm{r})} = 0$ and the initial covariance was selected as $\tilde{\Gamma}_{1|0}^{(\mathrm{r})} = \mathrm{diag}[(0.2\sigma_{\mathrm{bh}})^2, \ldots, (0.2\sigma_{\mathrm{bh}})^2, (10^{-6}\sigma_{\mathrm{bh}})^2]$. The standard deviation of the observation errors was assumed to be 0.4% of the difference between the maximum and minimum voltages, and the errors were assumed to be independent on each other. The state noise covariance was selected as $\tilde{\Gamma}_{wt}^{(\mathrm{r})} = \mathrm{diag}[\sigma_{\mathrm{bh}}^2, \ldots, \sigma_{\mathrm{bh}}^2, (10^{-7}\sigma_{\mathrm{bh}})^2]$. We also computed the Kalman filter estimates for comparison. In Kalman filter we used the same parameters as in fixed-lag smoother.

Fig. 3 shows a set of EIT reconstructions (Kalman filter and fixed-lag Kalman smoother) together with snapshots from the video. Since current injections and the images from the video do not correspond same instants of time, we present the 4th, 8th, ... and 40th video frames and closest reconstructed conductivity distributions. The reconstructions were rotated so that the impeller is in the same position as in the video snapshots even though they do not correspond exactly the same time instant as

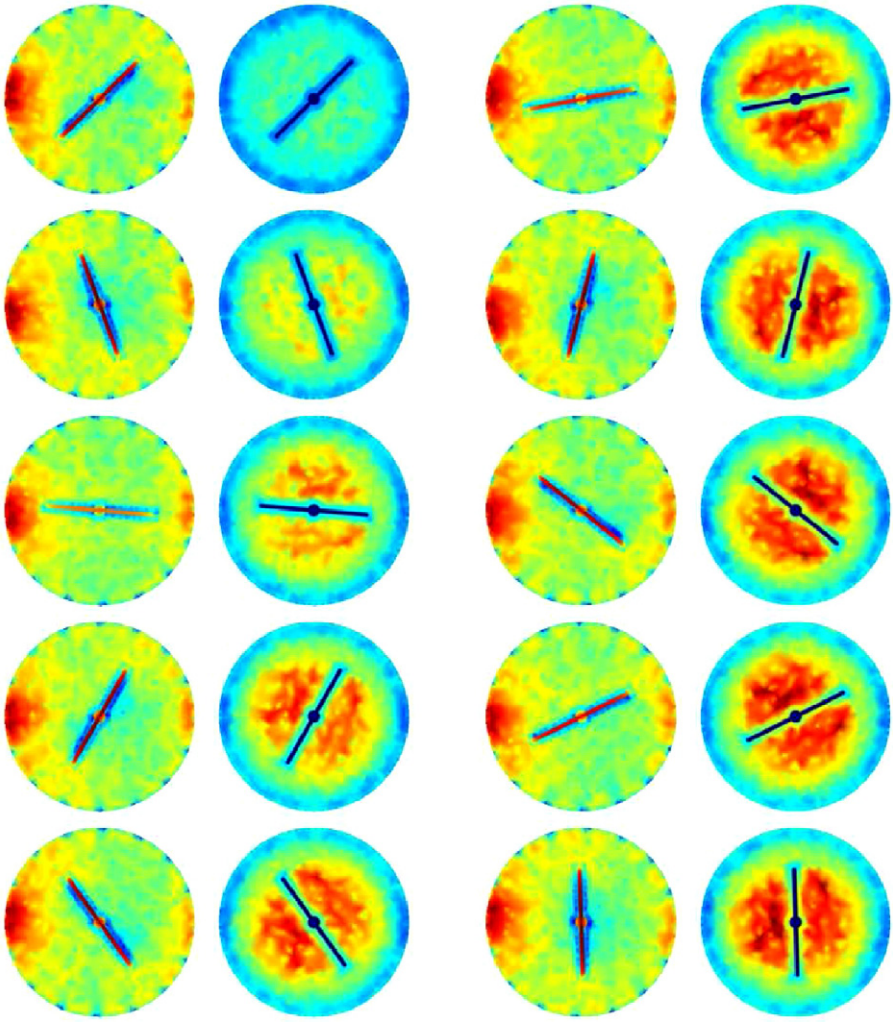

Fig. 4. Qualitative illustrations of sensitivity of EIT measurements (1st and 3rd column) and variances of the estimation errors related to the Kalman smoother estimates (2nd and 4th column). The figures correspond to the same time instants as in Fig. 3. Red color represents higher sensitivity and larger variance and blue color represents lower sensitivity and smaller variance.

the video snapshots. Both of the reconstructions are quite feasible, although the radial location of the resistive target (ball) is a bit inaccurate at certain times. Further, at certain time instants the ball is stretched in the reconstructions. This is due to the velocity gradients in the flow profile and the use of single-phase models to describe the evolution of the target. At some time instants the reconstructions may be almost solely based on the information given by the (single-phase) evolution model which is naturally not a very accurate model to describe the movement of a solid object. Especially, stretching effect occurs when the ball has traveled for some time in regions where the measurements are insensitive to changes in the conductivity. However, when the ball moves on and reaches a region with higher sensitivity the artefact due to the single-phase flow model diminishes. It should be noted that the fixed-lag Kalman reconstructions are computed using data also from the future and thus an estimate may suddenly become feasible even though the ball has not yet reached a sensitive region at that particular moment. This explains the minor difference between Kalman filter and Kalman smoother estimates. However, the quality of the Kalman filter reconstructions is not much lower than the quality of the Kalman smoother estimates.

The sensitivity of the measurements was analyzed by considering the Jacobian J_t. In order to find out which regions are sensitive to changes in the conductivity, we summed the rows of the absolute Jacobian at different time instants and plotted the values corresponding each nodal point of the mesh. The analysis showed that the regions with highest sensitivity are located in the close neighborhood of the current-injecting electrodes, especially close to the left most electrode, see Fig. 4. The sensitivity being higher in the neighborhood of the left-most electrode than in the neighborhood of the second current-injecting electrode, the rightmost electrode, is a result of using the left-most electrode as a ground electrode in voltage measurements. The position of the impeller seems to have quite a small effect on the sensitivity. However, sensitivity is slightly better near the tank wall on the regions close to the both ends of the impeller. In order to illustrate the accuracy of estimates we also plotted the variances of the estimation errors related to the fixed-lag Kalman smoohter estimates at different time instants, see Fig. 4. Starting from the initial value, the variances tend to become larger in the central area of the tank indicating that the accuracy of the estimates in lowest in this region. This is expectable since the central area suffers from low sensitivity.

6. Conclusions

In this paper non-stationary reconstruction methods with fluid dynamical models were tested with real EIT data. The quality of the state estimates was rather good taking into account that the target changed in such a high rate that all the stationary reconstruction schemes would have resulted useless estimates. One might criticize, however, the use of single-phase flow models in a case of multi-phase system. Indeed, the state estimates possess certain characteristic errors due to use of single-phase models. Furthermore, the observation and evolution processes were modeled using two-dimensional approximations. On the other hand, the fact that the state estimates are quite reliable even though the evolution model is somewhat biased is a very appealing result. In industrial applications the velocity field is never known accurately. The experimental results thus confirm the numerical results which suggested that the state estimates are relatively tolerant to mismodeling the velocity field [21].

The accuracy of the state estimates can further be improved by using (1) 3D observation model of EIT (note that even if the tank is flat, the 2D model is quite inaccurate), (2) non-linear state estimation scheme (such as iterated extended Kalman filter; linearization of the observation model of EIT naturally lowers the resolution), and (3) multi-phase flow model instead of CD model. All of these steps usually increase the computational cost of state estimation, and it depends on the application whether this additional cost can be tolerated. 3D modeling is required almost in all practical applications. In contrast, non-linear state estimation is not always necessary. However, in some off-line applications it may be reasonble. Similarly, in some off-line applications the use multi-phase flow models may be worthwhile.

References

[1] H.A. Nasr-El-Din, R.S. Mac Taggart, J.H. Masliyah, Local solids concentration measurement in a slurry mixing tank, Chem. Eng. Sci. 8 (1996) 1209–1220.
[2] R.M. West, X. Jia, R.A. Williams, Quantification of solid–liquid mixing using electrical resistance and positron emission tomography, Chem. Eng. Commun. 175 (1999) 71–97.
[3] M. Wang, A. Dorward, D. Vlaev, R. Mann, Measurement of gas–liquid mixing in a stirred vessel using electrical resistance tomography (ERT), Chem. Eng. J. 77 (2000) 93–98.
[4] S.M. Huang, A.B. Plaskowski, C.G. Xie, M.S. Beck, Tomographic imaging of two-component flow using capacitance sensors, J. Phys. E: Sci. Instrum. 22 (1989) 173–177.
[5] F.J. Dickin, R.A. Williams, M.S. Beck, Determination on composition and motion of multicomponent mixtures in process vessels using electrical impedance tomography. I. Principles and process engineering applications, Chem. Eng. Sci. 48 (1993) 1883–1897.
[6] T. Dyakowski, Process tomography applied to multi-phase flow measurement, Meas. Sci. Technol. 7 (1997) 343–353.
[7] J. Kaipio, P. Karjalainen, E. Somersalo, M. Vauhkonen, State estimation in time-varying electrical impedance tomography, Ann. N.Y. Acad. Sci. 873 (1999) 430–439.
[8] A. Seppänen, M. Vauhkonen, P. Vauhkonen, E. Somersalo, J. Kaipio, State estimation with fluid dynamical evolution models in process tomography—an application to impedance tomography, Inverse Probl. 17 (2001) 467–484.
[9] A. Seppänen, M. Vauhkonen, P. Vauhkonen, E. Somersalo, J. Kaipio, State estimation in three-dimensional impedance imaging. Use of fluid dynamical evolution models, in: Proceedings of Second World Congress on Industrial Process Tomography, 2001, pp. 198–206.
[10] P. Vauhkonen, M. Vauhkonen, T. Mäkinen, P. Karjalainen, J. Kaipio, Dynamical electrical impedance tomography—phantom studies, Inverse Probl. Eng. 8 (2000) 495–510.
[11] K. Kim, B. Kim, M. Kim, Y. Lee, M. Vauhkonen, Image reconstruction in time-varying electrical impedance tomography based on the extended Kalman filter, Meas. Sci. Technol. 12 (2001) 1032–1039.
[12] K. Kim, S. Kang, M. Kim, S. Kim, Y. Lee, M. Vauhkonen, Dynamic image reconstruction in electrical impedance tomography with known internal structures, IEEE Trans. Magn. 38 (2002) 1301–1304.

[13] E. Somersalo, M. Cheney, D. Isaacson, Existence and uniqueness for electrode models for electric current computed tomography, SIAM J. Appl. Math. 52 (1992) 1023–1040.
[14] M. Vauhkonen, Electrical Impedance Tomography and Prior Information, Ph.D. Thesis, University of Kuopio (1997).
[15] P. Vauhkonen, M. Vauhkonen, T. Savolainen, J. Kaipio, Three-dimensional electrical impedance tomography based on the complete electrode model, IEEE Trans. Biomed. Eng. 46 (1999) 1150–1160.
[16] A. Seppänen, State Estimation in Process Tomography, Ph.D. Thesis, University of Kuopio, Finland (2005).
[17] B.D.O. Anderson, J.B. Moore, Optimal Filtering, Prentice-Hall, 1979.
[18] T. Savolainen, L. Heikkinen, M. Vauhkonen, J. Kaipio, A modular adaptive electrical impedance tomography system, in: Proceedings of the Third World Congress in Industrial Process Tomography, Banff, Canada, 2003, pp. 3605–3609.
[19] L. Heikkinen, M. Vauhkonen, T. Savolainen, K. Leinonen, J. Kaipio, Electrical process tomography with known internal structures and resistivities, Inverse Probl. Eng. 9 (2001) 431–454.
[20] T.J. Chung, Computational Fluid Dynamics, Cambridge University Press, 2002.
[21] A. Seppänen, M. Vauhkonen, P.J. Vauhkonen, E. Somersalo, J.P. Kaipio, Fluid dynamical models and state estimation in process tomography: effect due to inaccuracies in flow fields, J. Electr. Imaging 10 (2001) 630–640.